ACS ES&T Engineering

pubs.acs.org/estengg

Article

Electrocoagulation Combined with Ultrafiltration Membranes as Pretreatment for RO Desalination of Synthetic Cooling Tower Blowdown Water

Kenji Lam,[♦] Erika Yamazaki,[♦] Rajuan Nelson, Sungsoon Kim, Jane Park, Javier A. Quezada-Renteria, Claire Murphy, Sandip Pal, Lily Lee, Xinyi Wang, Fan Yang, Minhao Xiao, Minju Cha, Costas Tsouris, Marta Hatzell, and David Jassby*

Cite This: https://doi.org/10.1021/acsestengg.5c00537

Read Online

ACCESS | Metrics & More | Article Recommendations

ABSTRACT: Electrocoagulation (EC), an electrochemical water treatment process, is commonly used to remove particulate and colloidal matter from water. Here, we demonstrate that EC, when coupled with membrane filtration, is also capable of removing dissolved species, such as Ca^{+}, Mg^{2+}, and SiO_x. The removal of such species is important for downstream membrane-based desalination treatment of the water that can suffer from reduced performance due to membrane scaling. Here, we describe how EC can be combined with a low-pressure membrane (LPM) system to offer efficient (and potentially universal) pretreatment for downstream membrane desalination. Synthetic water, simulating cooling tower blowdown (CTBD) with elevated concentrations of hardness and silicates (Ca: 418 ppm, Mg: 63 ppm, SiO_2: 50 ppm) is treated using EC coupled to ultrafiltration (UF) to remove Mg up to 30 ± 1%, Ca up to 29 ± 1%, and silica up to 99 ± 1%. We evaluated the effectiveness of the EC-UF pretreatment system in reducing downstream RO scaling using thermodynamic modeling to predict the saturation index (SI) at the RO membrane/water interface. An SI value below zero (SI < 0) indicates under-saturated conditions (with respect to a particular mineral) where mineral scaling does not take place, which correlates with improved water recovery. Our findings suggest that the EC-UF pretreatment system was able to increase water recovery by up to 30%, compared to 0% recovery without pretreatment, under optimal conditions (feed solution pH of 7 and an EC charge loading of 1800 C/L). Finally, we conducted an economic analysis showing that implementing an EC-UF system for CTBD water could yield a cost benefit of up to $14.13 per m^3 compared to direct brine disposal.

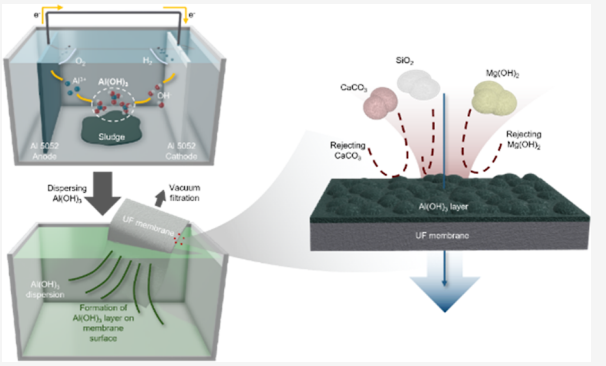

KEYWORDS: *hardness, silica, saturation index, membrane filtration, cooling tower blowdown*

1. INTRODUCTION

The power generation sector accounts for 41% of total domestic freshwater withdrawals, while also representing 6% of domestic consumptive use.[1,2] In power plants that practice water recycling, cooling water requires periodic discharge due to the gradual concentration of corrosion inhibitors, biocides, and antiscalants resulting from evaporation. This buildup can lead to scaling and equipment damage.[3] The discharged water, known as a cooling tower blowdown (CTBD) poses environmental concerns.[4] Treatment with reverse osmosis (RO) followed by reuse of CTBD as makeup water presents a promising solution, potentially reducing wastewater discharge and yielding significant water savings.[4] RO has become the predominant method for desalination due to its ability to achieve salt rejection exceeding 99% while being the more cost-effective compared to thermal-based desalination practices.[5,6]

RO systems face significant operational challenges, primarily due to membrane fouling and scaling.[7] Membrane fouling, caused by the accumulation of microorganisms and organic matter, and scaling, resulting from salt precipitation on the membrane surface, leads to increased operating pressures, reduced permeate quality, and membrane damage.[7,8] Various conventional pretreatment methods, such as pH adjustment and antiscalants have been utilized to tackle RO membrane scaling for the treatment of CTBD and other nontraditional water sources. However, these traditional approaches have

Received: June 18, 2025
Revised: August 19, 2025
Accepted: August 20, 2025

limitations, such as the risk of biofouling and corrosion of plant equipment, as well as increasing the treatment cost.[9] In addition, operators limit the % recovery through the RO membrane, with the goal of preventing the rejected salts from reaching supersaturated conditions, described by a saturation index (SI) > 0.[10] This practice limits the volume of recycled water and increases the volume of waste generated during the RO process.[11]

To address the challenges associated with conventional pretreatment methods for the treatment of CTBD, we explore an electrified, modular, and safe treatment process that integrates electrocoagulation (EC) and immersed membrane separation, with the goal of preparing the water for downstream RO desalination. EC systems consist of anodes and cathodes, typically made of aluminum and iron. When a voltage is applied, oxidation occurs at the anode, which results in metal dissolution and the release of metal ions (e.g., Al^{3+}); on the cathode, electrochemical reduction reactions occur, resulting in H_2 evolution and OH^- generation.[12] The ions produced from the sacrificial anode promote the coagulation of contaminants.[13]

Compared to conventional chemical coagulation (CC), EC offers significant advantages. It does not introduce additional ions such as chloride and sulfate, while demonstrating superior removal efficiency for total dissolved solids (TDS) and chemical oxygen demand (COD).[14] Critically, and in contrast to CC, EC does not change the pH of the water, whereas CC leads to the acidification of the stream.[15,16] It has also been established that EC can remove hardness and silica at a significantly lower cost compared to CC.[15]

Here we report the coupling of an EC system with an ultrafiltration (UF) membrane as a modular pretreatment approach, utilizing the safe, in situ generation of coagulants to enable downstream desalination of CTBD water. The synthetic CTBD used in this study contained high concentrations of scaling ions, particularly Ca (418 ppm), Mg (63 ppm), and silica (50 ppm), with a solution conductivity of 6.4 mS/cm. The use of UF membranes effectively removes larger contaminants such as bacteria, natural organic matter (NOM),[17] and oil droplets, as well as significantly enhance the removal of precipitated hardness and silicate.[18−20] Combining EC with an UF membrane offers improved mitigation of downstream RO fouling,[21] while enhancing the removal of certain contaminants such as heavy metals through cake-layer formation.[22] Additionally, immersing a membrane directly within the sedimentation tank of the EC system allows for the reduction of the system footprint.[23−25] The removal of hardness and silicate is evaluated in terms of their impact on the scaling of downstream RO membranes through the use of transport and thermodynamic modeling. Additionally, the removal mechanisms of hardness and silica in the EC and EC-UF systems are investigated using a mass balance approach, by quantitatively measuring the mass of each contaminant in the feed, effluent, floc, and on the cathode surface. An economic analysis is performed to evaluate the cost and benefits of EC-UF as pretreatment for RO, particularly in reducing the expenses associated with various RO brine disposal methods.

2. MATERIALS AND METHODS

2.1. Materials. 0.0813 cm thick 5052 aluminum alloy sheets were purchased from McMaster-Carr (Chicago, IL) and cut into 7.5 cm × 10 cm electrodes. NaCl, $MgSO_4·7H_2O$, $CaCl_2·2H_2O$, K_2SO_4, $NaNO_3$, $Na_2SiO_3·5H_2O$, BH_3O_3, Humic acid sodium salt, $NaHCO_3$, 67−70% HNO_3, 1N HCL, and 1N NaOH were obtained from Thermo Fisher Scientific (Waltham, MA). A synthetic CTBD solution (Table 1)[26] was prepared for all experiments, with the pH adjusted to pH 7, 8, and 9 using 1 N HCl and 1 N NaOH. A programmable direct current (DC) power supply (SPD3303X, Siglent Technologies NA, Inc., Solon, OH) operating under constant current conditions, was used to apply the potential to the electrode pair in the EC system, with charge loadings of 600 C/L, 1200 C/L, and 1800 C/L for these experiments. The EC unit used in this study, provided by WaterTectonics (Everett, WA), had dimensions of 15 cm × 10.2 cm × 10 cm. Membrane experiments utilized a commercial poly(ether sulfone) ultrafiltration membrane (PS-35) from Solecta, Inc. (Oceanside, CA). The membrane was housed in a poly(methyl methacrylate) membrane cassette (plate-and-frame) from Solter Plastics (Los Angeles, CA), which was immersed in the EC sedimentation tank. A Gast DOA-P704-AA vacuum pump (Gast Manufacturing, Inc., Benton Harbor, MI) was used to pull water through the membrane.

Table 1. Composition of Synthetic Cooling Tower Blowdown

chemical	concentration (mM)
NaCl	14.1
$MgSO_4·7H_2O$	2.6
$CaCl_2·2H_2O$	9.81
K_2SO_4	10.4
$NaNO_3$	2.47
$Na_2SiO_3·5H_2O$	0.832
BH_3O_3	0.463
Humic acid sodium salt	4.33
$NaHCO_3$	2

For membrane fabrication, polyvinylidene fluoride (PVDF) (761 Kaynar) and poly(methyl methacrylate) were generously supplied by Arkema Inc. (Torrance, CA). Glutaraldehyde, dodecyl benzenesulfonic acid, isopropyl alcohol (IPA) and dimethylacetamide (DMAC) were supplied by Sigma-Aldrich co. (ST. Louis, MO). Multiwalled carbon nano tubes (MWCNT) were sourced from Cheap Tubes Inc. (Grafton, VT).

2.2. PVDF and PVDF-CNT Membrane Fabrication. A solution containing 16 wt % PVDF and 2 wt % PMMA, was dissolved in DMAC at 80 °C for 8 h with stirring at 150 rpm, followed by placement in a desiccator for degassing for 6 h. Dope solutions were cast onto polypropylene fabric (Hollingsworth & Vose, East Warpole, MA) using a casting knife set at a thickness of 200 μm and then placed into a coagulation bath for 5 min. The coagulation bath contained water and IPA, with a water: IPA (volume/volume) ratio of 7:3. The PVDF membrane was removed from the coagulation bath, rinsed with DI water, and stored overnight in DI water.

MWCNTs were suspended in 1 L of deionized (DI) water at a concentration of 0.01 wt %. DDBS was added to the solution at a 1:10 CNT/DDBS ratio to enhance the dispersion of CNTs. The solution was then sonicated at 0 °C using a horn sonicator, pulsed in 1 s on and 1 s off intervals for a total of 30 min. Subsequently, the solution was centrifuged three times at 11,000 G and 4 °C for 10 min each to remove settled solids and ensure a homogeneous dispersion. The CNT: DDBS solution was transferred to a feed tank leading to an automated

https://doi.org/10.1021/acsestengg.5c00537
ACS EST Engg. XXXX, XXX, XXX−XXX

spray coater to coat a 12 cm × 10 cm PVDF ultrafiltration membrane that was made. The airbrush was positioned 15 cm above the membrane surface at a 90° angle. The apparatus was supported by infrared lights and heaters to prevent wetting of the membrane surface. Once coated, poly(vinyl alcohol) (PVA) was spray coated onto the membrane surface to achieve a PVA mass loading of 0.1 vol %. The PVDF-CNT membrane was then immersed in a cross-linking solution containing 1 g/L glutaraldehyde and 0.37 g/L of HCl (as a catalyst) at 80 °C for 1 h. Following this, the PVDF-CNT membrane was rinsed with DI water and dried at 90 °C for 5 min.

2.3. EC Experiment Procedure and Effluent Analysis. The total active area for the 5052 aluminum alloy sheets was 112 cm^2 from one anode and one cathode, placed 1 cm apart. The EC unit was continuously fed with synthetic CTBD solution at a flow rate of 0.1 L/min, where the hydraulic retention time was 42 s in the EC reactor. For each experiment, 2 L of CTBD solution was prepared and pumped through the EC cell for 20 min. The effluent was collected in a plastic bucket and allowed to rest for 24 h. To conduct a mass balance on the various species of interest in the feed stream (Ca, Mg, Si), the concentrations of these elements were evaluated in the EC effluent, the sedimented sludge, as well as any solids deposited on the cathode. To determine the mass of elements on the cathode, the used cathode was gently rinsed and dried. It was then placed in a glass Petri dish (McMaster-Carr, Chicago, IL) with 50 mL of 5 vol % HNO3 and soaked for 2 h to dissolve any scale deposited on the surface. The cathode was then removed from the Petri dish, and the remaining nitric acid was filtered through a 0.45 μm syringe filter (Tisch Scientific, Cleves, OH). The filtered nitric acid was diluted 20 times with DI water for IC analysis of Ca and Mg using a Dionex Integrion HPIC System (Thermo Fisher Scientific, Waltham, MA). The feed solution was gently stirred for even mixing and filtered through a 0.45 μm filter and diluted 10 times with DI water for IC analysis of Ca and Mg. 50 mL of the effluent was collected and filtered using a filtering flask with a 0.45 μm filter disc (Tisch Scientific, Cleves, OH). The filtered effluent was collected and diluted 10 times with DI water for IC analysis of Ca and Mg. The filter disc with the retained floc was gently rinsed with 10 mL of 5 vol % HNO3, which was collected and diluted 20 times with DI water for IC analysis of Ca and Mg. The same methodology was utilized for silica analysis using ICP-OES (iCAP PRO ICP-OES, Thermo Fisher Scientific, Waltham, MA).

2.4. Immersed Membrane Experiment Procedure and Effluent Analysis. The membrane cassette, with a membrane area of 0.2 m^2, was immersed into the EC effluent. A constant vacuum pressure of 0.9 bar was applied to the backside of the membrane to induce flux. The membrane was initially conditioned for 30 min with EC effluent. Subsequently, the experiment was run with the EC effluent for 210 min. Membrane flux was measured with a balance at 30 min intervals, and samples were collected at the same time intervals. Samples were then diluted 70 and 50 times for the feed and effluent, respectively, with DI water for IC analysis of Ca and Mg.

2.5. Sludge Characterization. Sedimented floc was filtered on a 0.45 μm filter disc and dried for 24 h in a vacuum oven. Energy dispersive spectroscopy (EDS) and scanning electron microscopy (SEM) imaging was conducted on the dried floc using a Phenom Pharos G2 desktop FEG-SEM (Thermo Fisher Scientific, Waltham, MA). The cross-section of the membrane foulant was imaged using Zeiss Supra 40VP SEM (ZEISS, Germany). Fourier transformed infrared (FTIR) analysis was performed using a Spectrum Two FTIR spectrometer (PerkinElmer, Waltham, MA), where 20 mg of the dried sludge was pressed into a pellet with 180 mg of KBr. X-ray photoelectron spectroscopy (XPS) analysis was carried out using a Kratos Axis Ultra DLD spectrometer with a monochromatic aluminum Kα X-ray source (Kratos Analytical Ltd., Manchester, UK) and analyzed using CasaXPS software (version 2.3.25). Floc was dried in an oven at 80 °C prior to XPS analysis.

2.6. RO Scaling Potential. Visual MINTEQ was utilized to calculate the saturation index (SI) of the main scaling salts at various water recoveries of a theoretical downstream RO membrane. Initially, the concentration factor, CF, and concentration polarization factor, CP, were calculated to accurately determine the limiting concentration factor for each specific ion species of interest, which was then used to determine the concentrations of the various ions at the RO membrane surface; the various variables used in these calculations are listed in Table 2. The limiting concentration factor (CF_{lim}) is the product of the concentration factor and concentration polarization factor[27,28]

$$CF_{lim} = CP \times CF \tag{1}$$

Table 2. Parameters for RO Model.[27]

symbol	value	units
Q_f	0.011	m^3s^{-1}
v_p	5.7×10^{-6}	ms^{-1}
ν	8.9×10^{-7}	m^2s^{-1}
r_s	0.994	
N_M	3	
N_L	31	
ε_{sp}	0.8	
W	0.7112	m
H^*	6.5×10^{-4}	m
d_H	0.001	m

To determine the CP factor, the local crossflow velocity, u_x is first determined by the equation below

$$u_x = \frac{Q_f}{N_M N_L \varepsilon_{sp} W H^*} \tag{2}$$

where Q_f is the feed flow rate, N_M is the number of RO membrane modules, N_L is the number of RO membrane elements, ε_{sp} is the spacer porosity number, W is the leaf width and H^* is the spacer thickness of the membrane.[27] For this study, it is assumed that the local crossflow velocity is equal to the inlet velocity, where the velocity is assumed to be constant across the whole RO membrane element. The Reynolds number (Re) along the membrane surface is calculated from the previously computed local crossflow velocity, u_x

$$Re = \frac{u_x d_H}{\nu} \tag{3}$$

where d_H is the channel hydraulic diameter and ν is the kinematic viscosity of the solution. The diffusivity (D) of each ion in the feed was determined from literature and is shown in the table below (Table 3).

https://doi.org/10.1021/acsestengg.5c00537
ACS EST Engg. XXXX, XXX, XXX−XXX

Table 3. Diffusivity of Ions in Synthetic Blowdown Water Solution.[29−34]

	diffusivity, $D\left(10^{-9}\frac{m^2}{s}\right)$
Na^+	1.33
Mg^{2+}	0.706
Ca^{2+}	0.792
K^+	1.96
B^{3+}	1.12
humic acid (TOC)	1.53
Cl^-	2.03
NO^{3-}	1.92
SO_4^{2-}	1.06
SiO_x	
CO_3^{2-}	0.80

The solute diffusivity values were then used to calculate the Schmidt Number, ($Sc = \nu/D$) for each individual ion. The Sherwood number, Sh, is calculated from the equation below

$$Sh = 0.065Re^{0.875}Sc^{0.25} \quad (4)$$

The mass transfer coefficient, k_s, is related to the Sherwood number, Sh, by the following equation

$$k_s = Sh\frac{D}{d_h} \quad (5)$$

The concentration polarization factor, CP, is estimated using the equation below

$$CP = \left[1 - r_s + r_s\exp\left(-\frac{v_p}{k_s}\right)\right]^{-1} \quad (6)$$

where $r_s = 1 - c_p/c_f$, is the observed solute rejection of the membrane and v_p is the water flux through the membrane. The concentration factor, CF, is determined by the equation below, where $Y = Q_p/Q_f$ is the product water recovery[27]

$$CF = \frac{1 - Y(1 - r_s)}{1 - Y} \quad (7)$$

The CF_{lim} is then multiplied by the initial feed solute concentrations to model the solute concentration at the RO membrane surface at water recoveries ranging from 60 to 90% at 10% increments. These concentrations were then used as input into Visual MINTEQ to calculate the SI of the main membrane scalants such as calcite, gypsum, and amorphous silica at the membrane/water interface. The SI in Visual MINTEQ is calculated using the formula below[35]

$$SI = \log\left(\frac{IAP}{K_{sp}}\right) \quad (8)$$

where IAP is the product of the activity of the participating ions in the precipitation reaction, and K_{sp} is the solubility product of the solid.[35]

2.7. Economic Analysis. A cost analysis was conducted for an EC-UF system, designed with a treatment capacity of 2352 m^3/day, based on the daily operational needs of a 300 MW power plant generator.[36] The system is assumed to have a lifespan of 30 years and was amortized over that period. The cost analysis compared the benefits of implementing an EC-UF pretreatment system followed by a downstream RO process, achieving reductions in brine disposal costs and water usage, against the alternative of disposing of CTBD water as untreated brine.

The savings from improved water recovery, WS ($/$m^3$), were calculated using the equation below, where R_0 is the water recovery in a system without EC-UF pretreatment and R_{ECM} is the water recovery in a system that is implementing EC-UF pretreatment. To calculate the savings achieved from improved water recovery with the EC-UF system, the equation below was used. The cost of makeup water, WC, ($1.49/$m^3$) is assumed to be the average industrial water rate in the west-pacific.[37]

$$WS = WC \times (R_{ECM} - R_0) \quad (9)$$

To calculate the cost savings for disposal of brine per m^3 of CTBD water treated using a RO process implementing the EC-UF pretreatment system, BD_{ECM} ($/$m^3$), the equation below was used. Where BD ($/$m^3$), is the cost to dispose of brine per m^3. All unrecovered CTBD water is assumed to be disposed of as brine.

$$BD_{ECM} = BD \times (R_{ECM} - R_0) \quad (10)$$

The capital cost (CAPEX) of the EC system was retrieved from literature and extrapolated for the system size using the 0.6 power rule.[38,39] The operating cost (OPEX) for the EC unit includes the price of replacing the electrodes and the cost of electricity that goes into electrode dissolution. The OPEX per unit volume of treated water can thus be expressed as follows[40]

$$OPEX_{EC} = aC_{electrode} + bC_{electricity} \quad (11)$$

where $C_{electricity}$ (kg/m^3) and $C_{electricity}$ (kWh/m^3) represent the quantity of electrode material and electricity consumed, respectively, and a ($/kg) and b($/kWh) are the associated unit prices. Parameter a corresponds to the price of an aluminum ingot (1.3 $/kg),[41] and the energy cost of aluminum sheet processing is 13 kWh/kg.[15] $C_{electricity}$ was obtained by calculating the energy demand of electrode dissolution using the following equation

$$E_{electrode\,dissolution} = \frac{I{\cdot}E{\cdot}t}{V} \quad (12)$$

where I is applied current (A), E is voltage (V), t is experiment duration (s), and $V$is the volume of treated water (m^3). Charge loading is represented by, $\frac{I{\cdot}t}{V}$ (C/L). E was recorded to be 4.5 V, at a charge loading of 1800 C/L.

The CAPEX and OPEX of the UF membrane system was calculated using a cost model retrieved from literature.[42] The exchange rate between Pound Sterling and United States Dollar used for this cost model is 1:0.745.[43]

The total cost of the EC-UF system, Total $Cost_{ECM}$ ($/$m^3$), was calculated using the equation below, applying an interest and discount rate of 3.0%, consistent with the 2025 federal discount rate for water resources planning as recommended by the U.S. Office of Management and Budget.[44] CAPEX was annualized using the Capital Recovery Factor (CRF),[45] and OPEX was discounted using the Annuity Present Value (APV)[46] as shown below, where i is the federal discount rate and n is the number of years over which the system is amortized. Both CAPEX and OPEX were then converted to units of $/$m^3$ for consistency.

https://doi.org/10.1021/acsestengg.5c00537
ACS EST Engg. XXXX, XXX, XXX−XXX

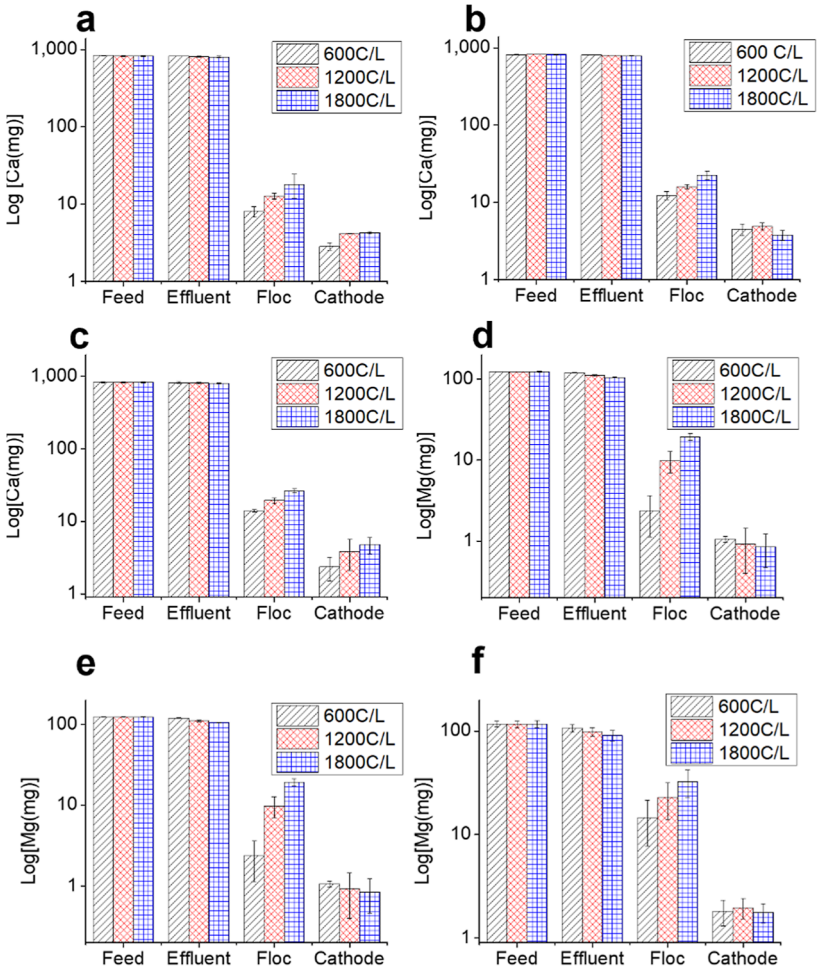

Figure 1. Mass balance for calcium at an initial pH of (a) pH = 7, (b) pH = 8, and (c) pH = 9. Magnesium mass balance at an initial pH of (d) pH = 7, (e) pH 8, (f) pH = 9. Three different charge loadings were analyzed (600, 1200, 1800 C/L).

$$\mathrm{CRF} = \frac{i(1+i)^n}{(1+i)^n - 1} \tag{13}$$

$$\mathrm{APV} = \frac{1-(1+i)^{-n}}{i} \tag{14}$$

$$\text{total cost}_{\mathrm{ECM}} = \mathrm{CAPEX}_{\mathrm{EC,CRF}} + \mathrm{CAPEX}_{\mathrm{UF,CRF}} + \mathrm{OPEX}_{\mathrm{EC,APV}} + \mathrm{OPEX}_{\mathrm{UF,APV}} \tag{15}$$

Finally, the cost savings/deficit ($/m^3) of implementing the EC-UF system was calculated by the equation below, where the difference between the savings achieved by reduced brine disposal cost and water consumption is compared against the cost of implementing the EC-UF system and a downstream RO process. The cost of implementing brackish water RO system is retrieved from literature as $0.3/m^3.[47]

$$\text{Cost benefit} = \mathrm{BD}_{\mathrm{ECM}} + \mathrm{WS} - \text{Total cost}_{\mathrm{ECM}} - 0.3 \tag{16}$$

3. RESULTS AND DISCUSSION

3.1. Charge Loading and Feed Water pH Effect on Hardness and Silica Removal. Coprecipitation has been hypothesized to be the mechanism responsible for the removal of hardness in EC. This occurs through excess OH^- production at the cathode, allowing for the local pH at the cathode surface to rise above 10, and resulting in the formation of calcium carbonate ($CaCO_3$), magnesium hydroxide ($Mg(OH)_2$) and magnesium carbonate ($MgCO_3$), which can be removed.[48] We hypothesize that the removal of hardness in EC is facilitated through the entrapment of Ca/Mg solids in aluminum floc. Despite this hypothesis, little work has confirmed this mechanism directly. Qualitative and quantitative analysis was performed to confirm this hypothesis.

We performed a mass balance to quantitatively account for where the hardness is removed. We specifically examined the inlet, effluent, cathode scaling material, and floc hardness content (Figure 1). Our results suggest that a significant portion of the hardness is removed through the floc, while only a minimal amount is removed through basic pH-induced precipitation at the cathode. The mass balance analysis indicates that varying the feedwater pH from 7 to 9 does not significantly affect the hardness removal mechanism in EC. This is likely because the removal mechanism involves the entrapment of precipitated Mg/Ca salts onto the generated floc. Therefore, the range of bulk pH values we explored here (which corresponds to typical natural water) does not significantly influence the formation of Mg/Ca salts, and the initial feedwater pH is not a significant factor. In contrast, increasing the charge loading changes the hardness removal through the EC floc significantly, where the Ca mass removal with the EC floc ranges from 11 ± 3 mg, 16 ± 3 mg, and 24 ±

https://doi.org/10.1021/acsestengg.5c00537
ACS EST Engg. XXXX, XXX, XXX−XXX

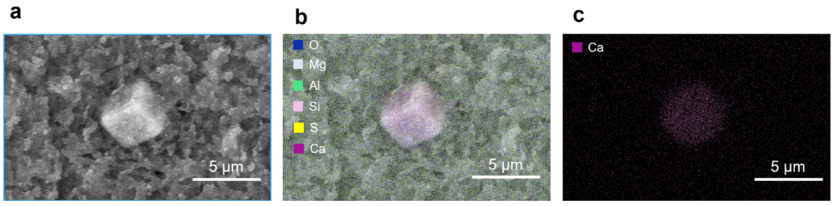

Figure 2. (a) SEM image of EC floc (b) EDS elemental analysis and mapping of EC floc. Including (c) Calcium. Calcium removal occurs through the entrapment of the crystals in the EC floc.

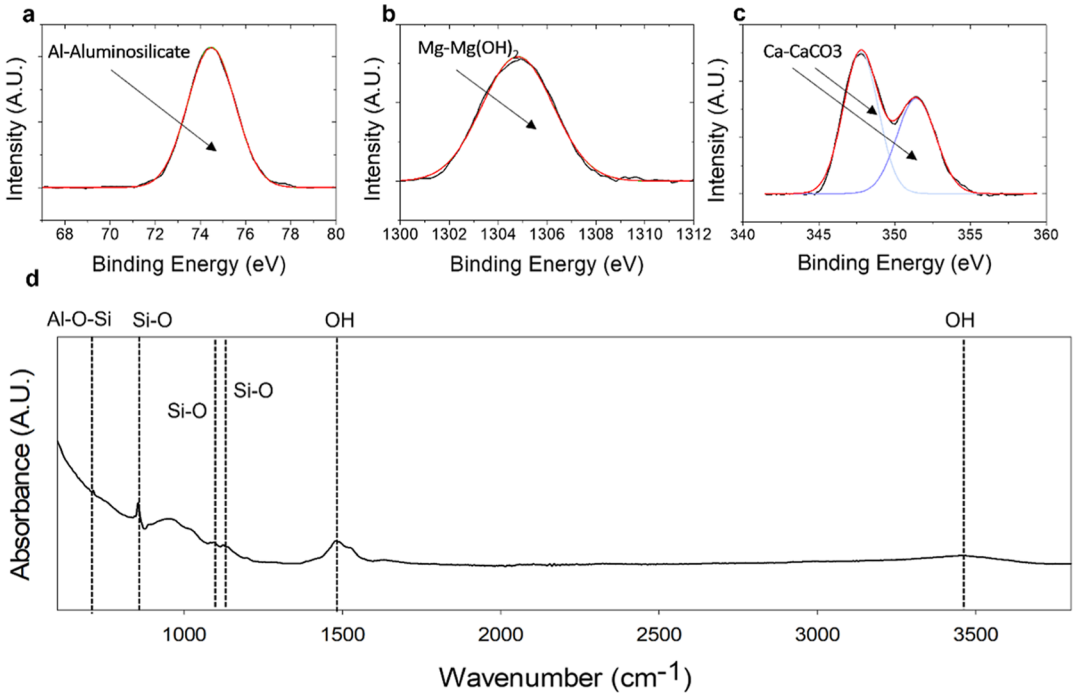

Figure 3. XPS analysis of EC floc. (a) Aluminum peaks (b) calcium peaks (c) magnesium peaks. (d) FTIR spectra of EC floc. Relevant Si, Al, O, and H bonds are labeled on the figure. FTIR pellets used for analysis were prepared with 150 mg of KBr and 20 mg of dried EC sludge.

3 mg, for 600 C/L, 1200 C/L, and 1800 C/L, respectively, while the Mg mass removal with the EC floc ranges from 8 ± 6 mg, 15 ± 8 mg, and 23 ± 9 mg, for 600 C/L, 1200 C/L, and 1800 C/L, respectively (Figure 1). This is a significant portion, compared to the cathode scale removal pathway where Ca mass removal through cathodic scaling ranges from 3.2 ± 1.1 mg, 4.3 ± 1 mg, and 4.2 ± 0.9 mg, for 600 C/L, 1200 C/L, and 1800 C/L, respectively, while the Mg mass removal with the cathodic scaling ranges from 1 ± 0.5 mg, 1.3 ± 0.6 mg, and 1.2 ± 0.5 mg, for 600 C/L, 1200 C/L, and 1800 C/L, respectively (Figure 1). This further reinforces the hypothesis that the majority of the hardness is removed through the entrapment of Mg/Ca solids in the EC floc. The increased charge loading is associated with more vigorous OH^- generation on the cathode, as well as to increased aluminum dissolution. The elevated OH^- concentrations can facilitate more $CaCO_3$ and Mg $(OH)_2$ solids formation, which are then captured and removed by the aluminum hydroxide floc. When considering the initial total mass of the Ca and Mg in the 2 L feed solution is 834 mg and 126 mg, the % removal with EC pretreatment alone does not exceed 4% for Ca and 21% for Mg—not a significant value considering the high initial Ca-based hardness levels. Therefore, further process modification would be required to enable meaningful hardness reduction. In our experiments, the charge loading did not have an appreciable impact on floc structure. Specifically, we did not observe any significant changes in floc structure from SEM imaging, membrane fouling behavior, or sedimentation times.

SEM imaging and EDS mapping show the presence of distinctive calcium-based crystals in the floc, suggesting that calcium is removed through physical entrapment (Figure 2). However, no distinct magnesium-based crystals were observed. XPS analysis of the floc showed the presence of $CaCO_3$ peaks[49] (Figure 3). In addition, $Mg(OH)_2$ peaks[50] were also observed in the XPS spectrum, suggesting a possible removal pathway through formation of $Mg(OH)_2$ during the EC process. It is possible that the flake-like structure of Mg $(OH)_2$ is not clearly observable in the SEM images due to their small size and complex floc structure. EDS imaging is also not able to accurately detect the small, dispersed structures of Mg $(OH)_2$ across the floc.

Silica removal was observed to be directly proportional to charge loading. (93 ± 3%, 98 ± 2%, and 99 ± 1% for 600 C/L, 1200 C/L, and 1800 C/L, respectively) (Figure 4). Similar to hardness removal, feed pH did not significantly affect silicate removal. We speculate that at higher charge loadings, increased electrode dissolution allows for the formation of more aluminosilicates, leading to a greater removal of silica mass.[51−53] The mechanism responsible for silica removal using aluminum electrodes in EC is proposed to involve the

https://doi.org/10.1021/acsestengg.5c00537
ACS EST Engg. XXXX, XXX, XXX−XXX

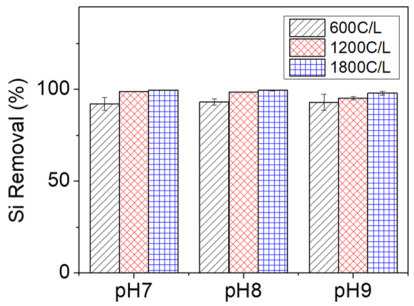

Figure 4. Silica percentage removal from synthetic CTBD at experimental conditions with pH 7, 8, 9 and charge loading of 600, 1200, 1800 C/L. Initial silica concentration of 50 mg/L. The retention time of the EC cell is 42 s, with a flow rate of 0.1 L/min. The concentration of Si in the feed and effluent water was measured by ICP-OES.

formation of aluminosilicates—a result of a reaction between hydrated silica and aluminum hydroxide flocs.[52] FTIR analysis of the EC floc supports this, showing an absorption band associated with Al−O−Si at around 700 cm^{-1} (Figure 3d).[15] The absorption band observed for Al−O−Si confirms that the removal of silica occurs through the coprecipitation of aluminosilicates from the hydrated silica present in the feed and aluminum aggregates produced within the EC chamber, a removal mechanism which has been extensively corroborated in the existing body of literature.[51−57] XPS analysis of the EC floc also shows a peak associated with aluminosilicate,[58] supporting the FTIR observations (Figure 3).

3.2. Effect of Scaling Mitigation in Downstream RO with an EC and EC-UF Pretreatment System. By combining EC and a downstream membrane filtration step, the SI of gypsum can be significantly reduced. The mechanism by which the membrane removes Ca and Mg salts involves the accumulation of these salts on the cake layer that forms on the membrane surface. This cake layer is created by the buildup of EC floc on the membrane. In all three membrane flux plots, there is a noticeable and dramatic decline in flux starting at 10 min of operation, relative to the initial flux measured at 5 min. This decrease in flux corresponds to the increase in hardness removal, which illustrates the importance of the fouling layer for enhanced hardness removal[59,60] (Figure 5). Beyond the initial rapid flux decline, the flux remains relatively stable for all 3 membranes used after 30 min. In these experiments, the flux declines from 123.7 ± 5 LMH, 156 ± 6 LMH, 170.4 ± 5.5 LMH at 5 min, to 62.1 ± 2.4 LMH, 78.2 ± 3.4 LMH, and 105.3 ± 3 LMH at 10 min, to stabilize at 52.8 ± 2 LMH, 71.5 ± 3.1 LMH, 98.8 ± 2.4 LMH after 30 min for PS-35, PVDF, and MWCNT-PVDF, respectively. After 210 min, the flux reaches 49.4 ± 4 LMH, 68.5 ± 1.9 LMH, 91.5 ± 1.2 LMH for PS-35, PVDF, and MWCNT-PVDF respectively.

In terms of the Ca removal through the membranes, the initial removal is 14.5 ± 0.5%, 12 ± 0.4%, 16 ± 0.3% at 5 min, 18.8 ± 0.4%, 17 ± 0.5%, 26.2 ± 0.6% at 30 min, and finally 20.3 ± 1%, 18.5 ± 0.8%, 28.6 ± 1% at 210 min for PS-35, PVDF, and MWCNT-PVDF, respectively. In terms of the Mg removal, the initial removal is 15.7 ± 0.4%, 13.7 ± 0.3%, 17.5 ± 0.3% at 5 min, 19.5 ± 0.7%, 18.6 ± 0.5%, 27.4 ± 0.7% at 30 min, and finally 21.5 ± 0.8%, 20.1 ± 1%, 30.3 ± 1% at 210 min for PS-35, PVDF, and MWCNT-PVDF, respectively. It is observed that the hardness rejection increases substantially between 5 and 30 min, by 4.3 to 12.8%, while the rejection only increases minimally, specifically by 1.4−2.9% from 30 to 210 min. From 5 to 30 min, the fouling layer is still forming,

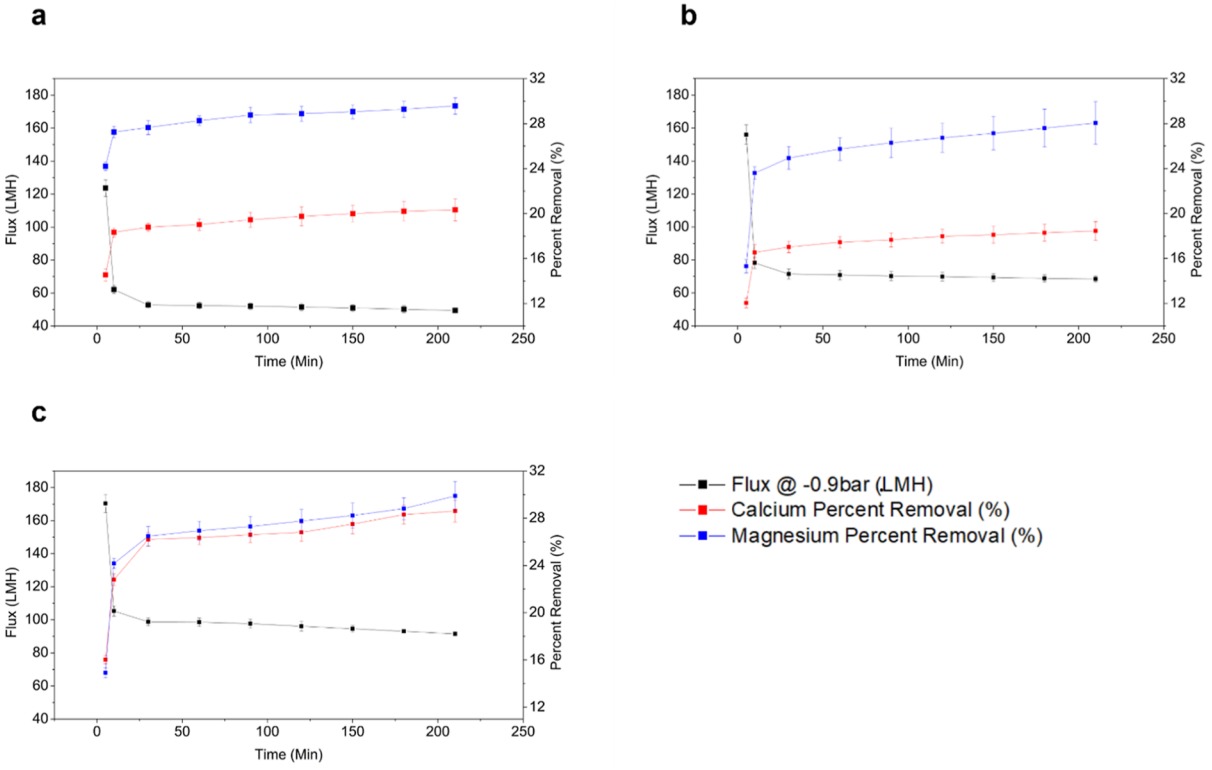

Figure 5. Flux and hardness removal plots for EC-UF pretreatment, where prior EC was conducted with a charge loading of 1800 C/L with a pH = 8 feed solution. (a) PS-35 (b) PVDF (c) MWCNT-PVDF.

https://doi.org/10.1021/acsestengg.5c00537
ACS EST Engg. XXXX, XXX, XXX−XXX

and as more foulant accumulates on the membrane surface, the rejection improves significantly. After 30 min, the fouling layer reaches a steady state where further accumulation of floc on the membrane surface is minimal, leading to only a slight improvement in hardness removal.

We hypothesize that the accumulation of the EC floc on the membrane surface creates an additional separation layer (i.e., cake layer filtration), where calcium and magnesium precipitates are captured. This hypothesis is supported by FTIR and XPS data, which show the presence of $CaCO_3$ and $Mg(OH)_2$ in the EC floc (Figure 3). The formation of $CaCO_3$ is likely due to the increased pH along the cathode surface, which drives the formation of $CaCO_3$.[61] While heterogeneous crystal growth of $CaCO_3$ on the cathode surface was observed, the majority of the $CaCO_3$ was found in the floc (Figure 1), and was likely formed from homogeneous precipitation in the bulk solution near the cathode surface, where the pH is still elevated. $Mg(OH)_2$ likely forms as excess hydroxide produced at the cathode combines with Mg^{2+} from the feed solution to form $Mg(OH)_2$.[62] To further confirm this hypothesis, SEM and EDS imaging were performed on the cross-section of the cake layer accumulated on the membrane (Figure 6). SEM images show crystal-like structures trapped on the surface of the EC floc layer. EDS mapping confirms that these structures are primarily composed of calcium, suggesting the presence of $CaCO_3$. Furthermore, a greater number of $CaCO_3$ precipitates were observed on the cake layer of the membrane compared to the EC floc. This is thought to occur because, as the membrane cake layer forms, it acts as an additional filter that more effectively traps small $CaCO_3$ precipitates, which require long settling times and are not effectively removed during conventional sedimentation during the EC process.

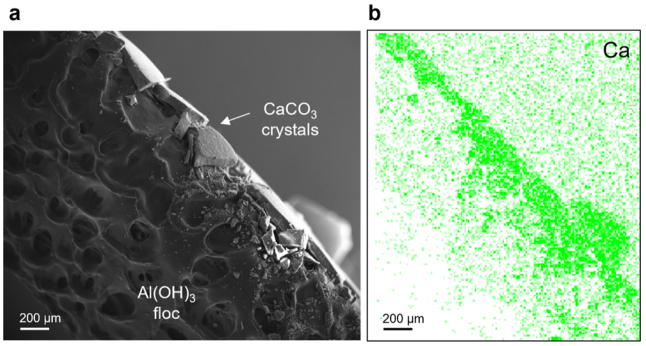

Figure 6. Cross-sectional (a) SEM image and (b) EDS Calcium analysis of membrane fouling layer. The foulant was collected and its cross-section was analyzed.

To assess the impact of EC and EC-UF system on downstream RO membrane scaling, the SI of amorphous silica (SiO_x), calcite ($CaCO_3$), and gypsum ($CaSO_4$) at a hypothetical downstream RO membrane/water interface was calculated as a function of water recovery in the RO system, with the EC and EC-UF treated CTBD as feed at a range of relevant pH values (pH 7, 8, and 9) (Figures 7, and 8). We only report these scalants, as they were identified by MINTEQ as the relevant scaling species in this system. The emergence of silicate scaling is dependent on the pH of the feed, the % recovery, and the charge loading (Figure 7a–c). Under all pH conditions, increasing the charge loading leads to higher Si removal, which reduces the SI at the membrane/water interface. At the lowest pH (7), a charge loading of 1800 C/L leads to sufficient silicate removal that allows water recovery to reach 50% before the SI > 0. At pH 8, the same charge loading (1800 C/L) allows for 40% recovery. However, lower charge loadings at these pH values do not remove enough silicate to prevent super saturation (Figure 7a–c). When the feed pH is 9, silicates are super saturated regardless of the charge loading. Considering that silicate removal is nearly complete from the EC effluent, these results demonstrate how sensitive RO membranes are to silicate scaling, particularly at elevated pH, and that the water would be difficult to desalinate without the addition of antiscalants or pH adjustment.

The impact of EC and EC-UF pretreatment on the SI of gypsum and calcite at the RO membrane/water interface were evaluated at a charge loading of 1800 C/L and feedwater pH of 8 (Figure 8a–d). EC pretreatment alone does not significantly affect the SIs of calcite and gypsum, consistent with EC's limited effectiveness in hardness removal. Gypsum scaling becomes an issue when recovery exceeds 40%, regardless of pH (as expected, since gypsum is not pH sensitive); calcite scaling is always an issue at all recoveries at pH8 (Figure 8d). While gypsum scaling is not impacted by the pH of the feed, it is highly dependent on the concentration of Ca. Although EC on

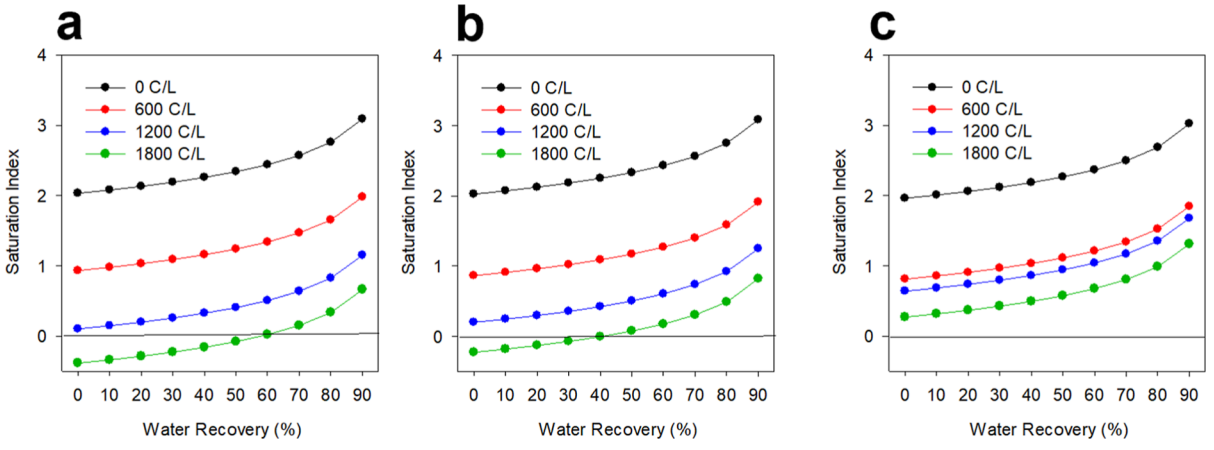

Figure 7. SI calculation of amorphous silica on a theoretical downstream RO membrane being fed effluent from the EC reactor at various experimental conditions. The SI was computed using Visual MINTEQ at various water recoveries from 0 to 90%, in 10% increments. The SI of amorphous silica of EC pretreated feedwater with charge loading of 0 C/L, 600 C/L, 1200 C/L, 1800 C/L at (a) pH = 7 (b) pH = 8 (c) pH = 9.

https://doi.org/10.1021/acsestengg.5c00537
ACS EST Engg. XXXX, XXX, XXX–XXX

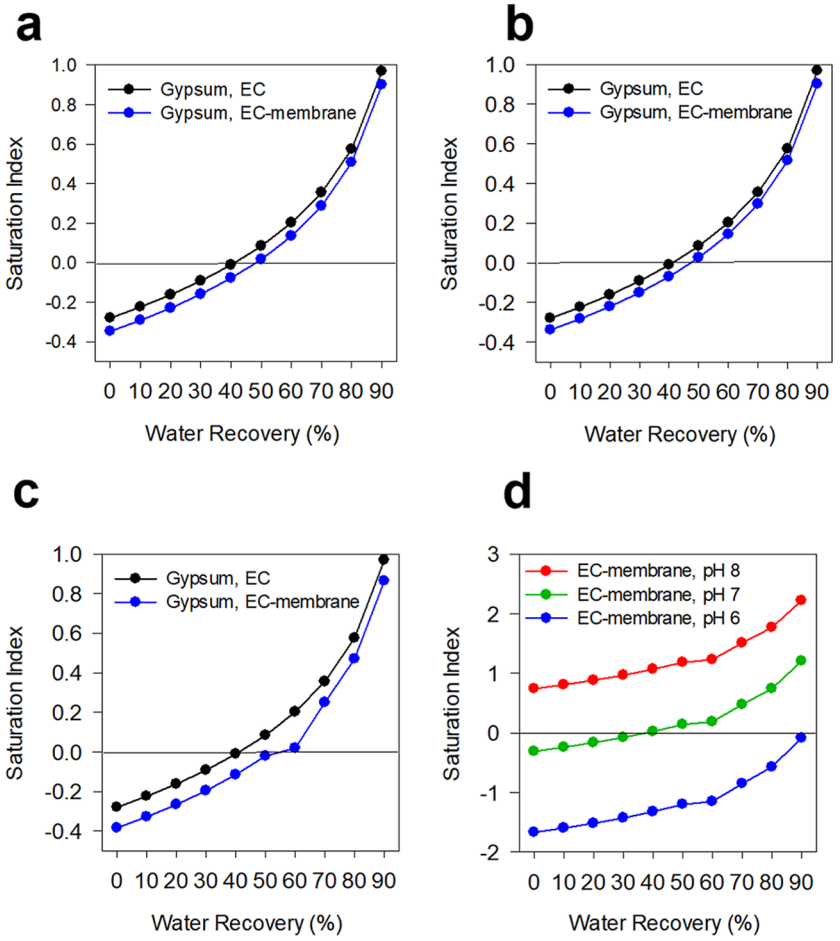

Figure 8. SI calculation of gypsum, and calcite on a theoretical downstream RO membrane being fed effluent from the EC/EC-UF reactor at various experimental conditions. The SI was computed using Visual MINTEQ at various water recoveries from 0 to 90%, in 10% increments. Comparison of SIs for calcite and gypsum between an EC pretreatment method and an EC-UF pretreatment method. (a) Gypsum SI comparison for PS-35 (b) Gypsum SI comparison for PVDF (c) Gypsum SI comparison for MWCNT-PVDF (d) Calcite SI in downstream RO utilizing MWCNT-PVDF effluent as feed. Calcite SI was simulated across pH 6 to 8 to investigate impact of pH adjustment on calcite scaling.

its own does not lead to significant Ca removal (Figure 1), the combination of EC with membrane filtration does lead to significant improvement in Ca removal (Figure 5). In general, enhanced Ca removal through the incorporation of membrane filtration manifested in a shift of SI toward higher recoveries, suggesting that the RO system can recover more water before it encounters scaling (Figure 8a–c). Specifically, the additional membrane step shifted the degree of water recovery before SI > 0 from 40% to 60%, when the MWCNT-PVDF membrane was used (the membrane that achieved the highest Ca removal) (Figure 8c). The other membranes evaluated in the study showed lower Ca removal, which resulted in only modest increases in possible water recoveries (Figure 8a,b).

At pH 8, the simulation shows that even with an EC-UF system utilizing MWCNT-PVDF membrane (highest Ca removal), conditions at the membrane/water interface are always super saturated (SI > 0) for calcite at a pH 8 with prior EC at 1800 C/L (Figure 8d). This is due to calcite's significantly lower solubility compared to gypsum (Ksp of 10^{-8}[48] vs 10^{-4}[58] for calcite and gypsum, respectively).[63,64] Therefore, Ca removal would have to increase to 95% under the current water chemistry at a pH of 8 to eliminate calcite scaling in downstream RO operating at 50% recovery. A common tactic used by operators to combat calcite scaling involves the acidification of the feed stream, which shifts the equilibrium concentrations of carbonate species toward bicarbonate ions (HCO_3^-), which do not participate in the formation of insoluble species.[65] Simulations were conducted at lower pH levels of 6 and 7 during EC-UF experiments, showing a significant reduction in calcite SI. At pH 7, the MWCNT-PVDF membrane achieved SI < 0 at a water recovery of 30%, while at pH 6, the calcite SI dropped below 0 at all water recoveries, allowing for 100% water recovery. These results demonstrate that calcite precipitation is highly dependent on pH, with even slight reductions significantly improving RO water recovery by minimizing calcite formation.

3.3. Economic Analysis of EC-UF System. A cost analysis was conducted to assess the impact of implementing an EC-UF system to reduce scaling and enhance water recovery in a downstream RO process treating CTBD water at a full-scale thermal power plant. The experimental work and SI simulations indicate that it would not be possible to recover any water with RO if the CTBD did not undergo some pretreatment to remove silicates and hardness. Therefore, our analysis considered the cost of the EC-UF pretreatment, which enabled a certain amount of water recovery using RO. RO retentate still requires disposal, which incurs an additional cost that is dependent on the disposal method. This cost (pretreatment + RO + brine disposal) was compared to the

https://doi.org/10.1021/acsestengg.5c00537
ACS EST Engg. XXXX, XXX, XXX−XXX

cost of brine disposal for the base-case where no RO was possible (i.e., all the CTBD requires disposal).

The experimental results and SI simulations identified that the optimal operating conditions for the EC-UF system with a downstream RO process are at an EC charge loading of 1800 C/L, a pH of 7, and a water recovery of 30%. Among the three major scalants (calcite, gypsum, and amorphous silica), calcite formation is the limiting factor for the system's water recovery post EC pretreatment. Under optimal conditions, the SI of calcite is less than 0 at a 30% water recovery. However, if calcite is not present, and the other scalants are considered, the system could achieve a water recovery of up to 40%. The pH of 7 was selected because most of the water to be treated will naturally fall around this value, although a lower pH would limit calcite scaling and enable higher water recovery.[66]

The cost-savings/deficits are calculated using eq 16, where the costs of implementing the EC-UF system and a downstream RO process are compared against the savings achieved by reduction in water use and RO brine disposal costs. The cost analysis will show a positive value if the cost-savings from implementing the EC-UF/RO system under optimal experimental conditions (1800 C/L at pH 7) exceed the costs associated with disposing of all CTBD water using alternative brine disposal methods. Conversely, a negative value representing a cost deficit would be shown if these savings were less than the disposal costs (Figure 9).

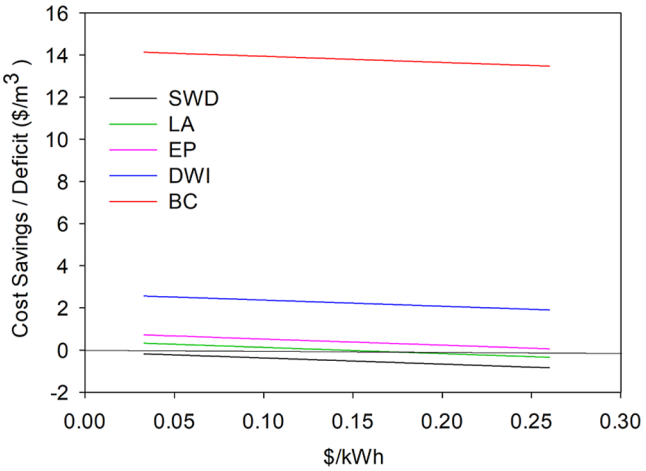

Figure 9. Cost savings/deficit of implementing EC-UF pretreatment per m^3 of CTBD water treated with RO is compared to the cost of disposing of all CTBD water as brine, using various brine disposal methods against the cost of electricity ($/kWh). A positive value indicates cost savings achieved by implementing the EC-UF system, while a negative value indicates a cost deficit associated with its implementation, when compared to just disposing of CTBD as brine. Brine disposal methods compared are surface water discharge (SWD), land application (LA), evaporation ponds (EP), deep-well injection (DWI), and brine crystallizer (BC).

The costs of the disposal methods per m^3 of brine were obtained from literature,[67−69] and listed as follows: surface water discharge (SWD) \$0.3/m^3, land application (LA) \$1.95/m^3, evaporation ponds (EP) \$3.28/m^3, deep-well injection (DWI) \$9.4/m^3, and brine crystallizer (BC) \$26/m^3. SWD is the lowest cost disposal method, where brine is discharged directly into open bodies of water, such as the ocean, a rivers, or a lake, although this kind of discharge is becoming increasingly rare due to the adverse environmental impacts associated with the introduction of brines into the aquatic environment.[67] DWI involves injecting brine into deep, porous rock formations, where the injected water is isolated from drinking water aquifers.[67] The cost of DWI used in this analysis is based on a previous study investigating the use of DWI in the Barnett Shale region of Texas.[69] DWI injection sites are relatively sparse, sometimes requiring water to be transported over considerable distances, which significantly increases costs. In this analysis, a transportation distance of approximately 60 miles is assumed,[69] as it provides a reasonable representation of typical conditions. Shorter distances would result in lower costs, while longer distances would lead to higher expenses. Given that there are only 800 Class I wells in the U.S. permitted for hazardous and nonhazardous waste injection, the transportation of CTBD to an injection site must be factored into the analysis—unless a suitable well happens to be located on-site at the power plant. LA is a method of disposing of brine by irrigating salt-tolerant vegetation. However, its large-scale use is limited by factors such as climate conditions and the water demand for irrigation. In addition, there are concerns with this approach as CTBD may contain elevated concentrations of heavy metals, which can lead to soil degradation over time.[70] EP is a method where brine is usually transported via pipelines to shallow, lined ponds and allowed to evaporate under ambient conditions.[67,71] While effective, these ponds require constant maintenance to avoid leakage and can present a hazard to migratory birds and other wildlife.[67] BC is achieved using several different forced evaporative methods, such as mechanical vapor compression, or multieffect distillation, where water is constantly evaporated (and sometimes condensed and reused) and the resulting salt crystals are separated and collected.[72]

As the EC-UF/RO process only relies on electricity as a continuous input, a sensitivity analysis around the cost of electricity was conducted. The current industrial electricity rate in CA (\$0.26/kWh)[73] was used as the costliest scenario, resulting in a total cost of \$1.08/m^3 of CTBD feedwater for implementing the EC-UF/RO system. The addition of the EC-UF/RO system offers a financial advantage compared to the more expensive brine disposal methods such as EP, DWI, and BC. Specifically, the cost savings gained per m^3 of CTBD water treated are \$0.06/m^3, \$1.9/m^3, and \$13.47/m^3, compared to DWI, and BC, respectively (Figure 9). However, when compared to cheaper disposal methods such as EP, and LA, these methods are cheaper than the EC-UF/RO by \$0.34/m^3, and \$0.84/m^3, respectively (Figure 9). However, these cheaper methods come with drawbacks, such as harming the receiving water body's ecosystem, contaminating groundwater aquifers, and limitations on large-scale implementations.[67]

Cheaper energy sources such as offshore wind (\$0.075/kWh), hydropower (\$0.057/kWh), solar (\$0.044/kWh), and onshore wind (\$0.033/kWh) were also considered for powering the EC-UF/RO system.[74] For offshore wind energy, the total cost of operating the EC-UF/RO system is \$0.54/m^3, where the cost savings gained per m^3 of CTBD water treated are \$0.2/m^3, \$0.59/m^3, \$2.44/m^3, and \$14.01/m^3, compared to LA, EP, DWI, and BC, respectively (Figure 9). When compared to cheaper disposal methods such as SWD, this method is cheaper than the EC-UF/RO by \$0.3/m^3 (Figure 9). For hydropower, the total cost of operating the EC-UF/RO system is \$0.48/m^3, where the cost savings gained per m^3 of CTBD water treated are \$0.25/m^3, \$0.65/m^3, \$2.49/m^3, and \$14.06/m^3, compared to LA, EP, DWI, and BC, respectively

https://doi.org/10.1021/acsestengg.5c00537
ACS EST Engg. XXXX, XXX, XXX−XXX

(Figure 9). When compared to cheaper disposal methods such as SWD, this method is cheaper than the EC-UF/RO by \$0.25/m^3 (Figure 9). For Solar, the total cost of operating the EC-UF/RO system is \$0.45/m^3, where the cost savings gained per m^3 of CTBD water treated are \$0.29/m^3, \$0.68/m^3, \$2.53/m^3, and \$14.1/m^3, compared to LA, EP, DWI, and BC, respectively (Figure 9). When compared to cheaper disposal methods such as SWD, this method is cheaper than the EC-UF/RO by \$0.21/m^3 (Figure 9). Finally, using onshore wind energy (\$0.033/kWh), the recalculated total cost of the EC-UF/RO system is \$0.41/m^3. Specifically, it allows for cost savings gained per m^3 of CTBD of \$0.32/m^3, \$0.72/m^3, \$2.56/m^3, and \$14.13/m^3, compared to LA, EP, DWI, and BC, respectively (Figure 9). Although the system is still not financially competitive with SWD—showing a cost deficit of \$0.18/m^3—the deficits are reduced by a factor of 4 compared to calculations based on California's industrial electricity rate (Figure 9).

The cost savings from using renewable energy sources make the implementation of EC-UF systems feasible for a wider range of brine disposal methods, while further improving the cost savings for methods that are already viable. Figure 9 highlights that the breakeven electricity price for achieving cost savings with the EC-UF/RO system, when paired with LA, is \$0.14/kWh. With electricity costs below this threshold, the system becomes economically advantageous. This makes offshore wind, hydropower, solar energy, and onshore wind, particularly attractive options, as their costs are already below \$0.14/kWh. By leveraging renewable energy sources, the overall cost of implementing the EC-UF system is significantly reduced, since the majority of its operating expenses stem from the electricity required for the EC process. Hence, the EC-UF system could be implemented in a cost-effective manner in areas with no availability of SWD sites by improving water recovery and using renewable energy to sustainably reduce brine disposal costs.

4. CONCLUSIONS

Here we examined an EC system coupled with an immersed UF membrane for the pretreatment of CTBD prior to an RO desalination process. The majority of the hardness removal in EC occurs through the entrapment of $CaCO_3$ and Mg $(OH)_2$ salts in the aluminum hydroxide flocs generated during EC; silica removal occurs through the formation and coprecipitation of aluminosilicates. The variation in feed pH at 7, 8, and 9 for EC did not significantly affect the removal of hardness and silica. However, increasing the charge loading from 600 C/L to 1800 C/L for EC improved the removal of Ca, Mg, and Si via EC by 54%, 65%, and 6%, respectively. EC can remove nearly all of the silica at sufficiently high charge loading but is significantly less effective at hardness removal. However, by integrating EC with an immersed UF membrane step, we observed a considerable improvement in hardness removal. Specifically, the Ca and Mg removal increased by 90% and 40% respectively. The EC floc forms a fouling layer on the UF membrane and acts as an additional separation layer that can better retain the smaller $CaCO_3$ and Mg $(OH)_2$ crystals which were not removed by sedimentation in the EC cell. SI simulations using the water chemistry in this study show that this system is able to reduce the SI of gypsum and amorphous silica significantly, while calcite scaling needs to be managed through pH adjustments. An economic analysis was conducted to assess the feasibility of implementing EC-UF/RO at the optimum experimental conditions identified for treating CTBD water in a full-scale thermal power plant. A sensitivity analysis around the cost of electricity demonstrated that implementing an EC-UF/RO process at a full-scale thermal power plant can offer significant cost savings per m^3 of CTBD treated, compared to traditional brine disposal methods. Under optimal conditions (EC charge loading of 1800 C/L, pH 7, and 30% water recovery), and at the current California industrial electricity rate, the EC-UF/RO system provides cost savings, especially when compared to high-cost disposal options such as DWI, BC, and EP (\$0.06/m^3, \$1.9/m^3, and \$13.47/m^3 respectively). For the cheapest form of renewable energy, onshore wind, cost savings are also achieved for LA at \$0.32/m^3, combined with increased cost savings for DWI, BC, and EP (\$0.72/m^3, \$2.56/m^3, and \$14.13/m^3, respectively). While cheaper disposal methods such as LA and SWD may initially seem more cost-effective, they come with significant environmental and practical limitations, which can make them unsuitable for large-scale or long-term use. The EC-UF/RO system, although more expensive than these methods, offers a more sustainable and efficient solution that enhances water recovery and reduces brine disposal costs. Overall, the integration of the EC-UF/RO system, particularly when paired with renewable energy sources, presents a promising solution for improving water recovery and sustainably managing brine disposal in power plants, offering both environmental and economic benefits.

AUTHOR INFORMATION

Corresponding Author

David Jassby − *Department of Civil & Environmental Engineering, University of California, Los Angeles, Los Angele, California 90095, United States; UCLA California NanoSystems Institute, Los Angeles, California 90095, United States; UCLA Institute of the Environment & Sustainability, Los Angeles, California 90095, United States;* orcid.org/0000-0002-2133-2536; Email: jassby@ucla.edu

Authors

Kenji Lam − *Department of Civil & Environmental Engineering, University of California, Los Angeles, Los Angele, California 90095, United States;* orcid.org/0009-0003-7573-4842

Erika Yamazaki − *School of Chemical & Biomolecular Engineering, Georgia Institute of Technology, Atlanta, Georgia 30332-0100, United States*

Rajuan Nelson − *Department of Civil & Environmental Engineering, University of California, Los Angeles, Los Angele, California 90095, United States*

Sungsoon Kim − *Department of Civil & Environmental Engineering, University of California, Los Angeles, Los Angele, California 90095, United States*

Jane Park − *Department of Chemical and Biomolecular Engineering, University of California, Los Angeles, California 90095, United States*

Javier A. Quezada-Renteria − *Department of Civil & Environmental Engineering, University of California, Los Angeles, Los Angele, California 90095, United States*

Claire Murphy − *Department of Materials Science and Engineering, University of California, Los Angeles, Los Angeles, California 90095, United States*

https://doi.org/10.1021/acsestengg.5c00537
ACS EST Engg. XXXX, XXX, XXX−XXX

Sandip Pal − *Department of Civil & Environmental Engineering, University of California, Los Angeles, Los Angele, California 90095, United States*
Lily Lee − *Department of Civil and Environmental Engineering, Imperial College London, London SW7 2AZ, U.K.*
Xinyi Wang − *Department of Civil & Environmental Engineering, University of California, Los Angeles, Los Angele, California 90095, United States*
Fan Yang − *Department of Civil & Environmental Engineering, University of California, Los Angeles, Los Angele, California 90095, United States;* orcid.org/0000-0001-6319-6053
Minhao Xiao − *Department of Civil & Environmental Engineering, University of California, Los Angeles, Los Angele, California 90095, United States*
Minju Cha − *Department of Civil & Environmental Engineering, University of California, Los Angeles, Los Angele, California 90095, United States;* orcid.org/0000-0002-1985-6074
Costas Tsouris − *Manufacturing Science Division, Oak Ridge National Laboratory, Oak Ridge, Tennessee 37831, United States;* orcid.org/0000-0002-0522-1027
Marta Hatzell − *George W. Woodruff School of Mechanical Engineering, Georgia Institute of Technology, Atlanta, Georgia 30332, United States;* orcid.org/0000-0002-5144-4969

Complete contact information is available at: https://pubs.acs.org/10.1021/acsestengg.5c00537

Author Contributions

♦K.L. and E.Y. are cofirst authors.

Notes

The authors declare no competing financial interest.

■ ACKNOWLEDGMENTS

Support for this work was provided by the National Alliance for Water Innovation (NAWI), funded through the US Department of Energy (DOE), Office of Energy Efficiency and Renewable Energy (EERE), Advanced Manufacturing Office, under Funding Opportunity Announcement RP20407-003. SEM and EDS data acquisition was performed on the Zeiss Supra 40VP SEM by Judy Su at the Electron Imaging Center for Nanosystems (EICN) at the University of California, Los Angeles's California for NanoSystems Institute (CNSI), RRID:SCR_022900.

■ REFERENCES

(1) Nair, S.; Timms, W. Freshwater Footprint of Fossil Fuel Production and Thermal Electricity Generation and Water Stresses across the National Electricity Market (NEM) Region of Australia. *J. Cleaner Prod.* **2020**, *267*, 122085.
(2) Talati, S.; Zhai, H.; Kyle, G. P.; Morgan, M. G.; Patel, P.; Liu, L. Consumptive Water Use from Electricity Generation in the Southwest under Alternative Climate, Technology, and Policy Futures. *Environ. Sci. Technol.* **2016**, *50* (22), 12095−12104.
(3) Wagner, T. V.; Parsons, J. R.; Rijnaarts, H. H. M.; de Voogt, P.; Langenhoff, A. A. M. A Review on the Removal of Conditioning Chemicals from Cooling Tower Water in Constructed Wetlands. *Crit. Rev. Environ. Sci. Technol.* **2018**, *48* (19−21), 1094−1125.
(4) Jain, R.; Nigam, H.; Mathur, M.; Malik, A.; Arora, U. K. Towards Green Thermal Power Plants with Blowdown Water Reuse and Simultaneous Biogenic Nanostructures Recovery from Waste. *Resour., Conserv. Recycl.* **2021**, *168*, 105283.
(5) Liu, Z.; Zhang, S.; Kilburn, Z. J. Thermodynamic and Economic Analysis of Reverse Osmosis and Multi-Effect Thermal Vapor Compression Desalination Systems: A Comparative Study. *Desalin. Water Treat.* **2021**, *220*, 36−52.
(6) Kim, S.; Choi, H.; Kim, B.; Lim, G.; Kim, T.; Lee, M.; Ra, H.; Yeom, J.; Kim, M.; Kim, E.; Hwang, J.; Lee, J. S.; Shim, W. Extreme Ion-Transport Inorganic 2D Membranes for Nanofluidic Applications. *Adv. Mater.* **2023**, *35* (43), 2206354.
(7) Goh, P. S.; Lau, W. J.; Othman, M. H. D.; Ismail, A. F. Membrane Fouling in Desalination and Its Mitigation Strategies. *Desalination* **2018**, *425*, 130−155.
(8) Alshami, A.; Taylor, T.; Ismail, N.; Buelke, C.; Schultz, L. RO System Scaling with Focus on the Concentrate Line: Current Challenges and Potential Solutions. *Desalination* **2021**, *520*, 115370.
(9) Anis, S. F.; Hashaikeh, R.; Hilal, N. Reverse Osmosis Pretreatment Technologies and Future Trends: A Comprehensive Review. *Desalination* **2019**, *452*, 159−195.
(10) Bystrianský, M.; Nir, O.; Šír, M.; Honzajková, Z.; Vurm, R.; Hrychová, P.; Bervic, A.; van der Bruggen, B. The Presence of Ferric Iron Promotes Calcium Sulphate Scaling in Reverse Osmosis Processes. *Desalination* **2016**, *393*, 115−119.
(11) Li, X.; Hasson, D.; Semiat, R.; Shemer, H. Intermediate Concentrate Demineralization Techniques for Enhanced Brackish Water Reverse Osmosis Water Recovery - A Review. *Desalination* **2019**, *466*, 24−35.
(12) Shahedi, A.; Darban, A. K.; Taghipour, F.; Jamshidi-Zanjani, A. A Review on Industrial Wastewater Treatment via Electrocoagulation Processes. *Curr. Opin. Electrochem.* **2020**, *22*, 154−169.
(13) Castañeda, L. F.; García, I.; Nava, J. L.; Coreño, O. Concurrent Arsenic, Fluoride, and Hydrated Silica Removal from Deep Well Water by Electrocoagulation: Comparison of Sacrificial Anodes (Al, Fe, and Al-Fe). *J. Environ. Manage.* **2024**, *365*, 121597.
(14) Das, P. P.; Sharma, M.; Purkait, M. K. Recent Progress on Electrocoagulation Process for Wastewater Treatment: A Review. *Sep. Purif. Technol.* **2022**, *292*, 121058.
(15) Liu, Y.-H.; Bootwala, Y. Z.; Jang, G. G.; Keum, J. K.; Khor, C. M.; Hoek, E. M. V.; Jassby, D.; Tsouris, C.; Mothersbaugh, J.; Hatzell, M. C. Electroprecipitation Mechanism Enabling Silica and Hardness Removal through Aluminum-Based Electrocoagulation. *ACS EST Eng.* **2022**, *2*, 1200.
(16) Khor, C. M.; Liao, M. E.; Iddya, A.; Ma, S.; Yang, F.; Liu, Y.-H.; Bootwala, Y. Z.; Jang, G. G.; Goorsky, M. S.; Hoek, E. M. V.; Tsouris, C.; Mothersbaugh, J.; Hatzell, M. C.; Jassby, D. Physical and Electrochemical Characterization of Aluminum Electrodes during Electrocoagulation. *ACS EST Water* **2024**, *4* (1), 44−56.
(17) Zhu, X.; Jassby, D. Electroactive Membranes for Water Treatment: Enhanced Treatment Functionalities, Energy Considerations, and Future Challenges. *Acc. Chem. Res.* **2019**, *52* (5), 1177−1186.
(18) Virga, E.; Field, R. W.; Biesheuvel, P. M.; de Vos, W. M. Theory of Oil Fouling for Microfiltration and Ultrafiltration Membranes in Produced Water Treatment. *J. Colloid Interface Sci.* **2022**, *621*, 431−439.
(19) Shemer, H.; Melki-Dabush, N.; Semiat, R. Removal of Silica from Brackish Water by Integrated Adsorption/Ultrafiltration Process. *Environ. Sci. Pollut. Res.* **2019**, *26* (31), 31623−31631.
(20) Xu, B.; Zhang, Q.; Wu, H.; Tian, Q.; Chai, W.; Zhang, M.; Shao, G.; Tian, S.; Lin, Y.; Yao, H. Integrated Membrane Process of Tubular Ultrafiltration-Nanofiltration-Electrodialysis-Reverse Osmosis for Treating Fracturing Flowback Fluid. *J. Cleaner Prod.* **2024**, *469*, 142995.
(21) Tahreen, A.; Jami, M. S.; Ali, F. Role of Electrocoagulation in Wastewater Treatment: A Developmental Review. *J. Water Process Eng.* **2020**, *37*, 101440.
(22) Niu, B.; Mao, Z.; Liang, D.; Liao, Y.; Zhang, M.; Meng, S. *The Surprising Role of Fouling Layer in Removal of Heavy Metals During Ultrafiltration Benefiting from Their Binding with Organic Foulants*;

Social Science Research Network: Rochester, NY, 2025. (accessed 2024−12−04).
(23) Moneer, A. A. The Potential of Hybrid Electrocoagulation-Membrane Separation Processes for Performance Enhancement and Membrane Fouling Mitigation: A Review. *Egypt. J. Aquat. Res.* **2023**, *49* (3), 269−282.
(24) Lee, M.; Wu, Z.; Li, K. 2—Advances in Ceramic Membranes for Water Treatment. In *Advances in Membrane Technologies for Water Treatment*; Basile, A., Cassano, A., Rastogi, N. K., Eds.; *Woodhead Publishing Series in Energy*; Elsevier: Oxford, 2015; pp 43−82..
(25) Othman, N. H.; Alias, N. H.; Fuzil, N. S.; Marpani, F.; Shahruddin, M. Z.; Chew, C. M.; David Ng, K. M.; Lau, W. J.; Ismail, A. F. A Review on the Use of Membrane Technology Systems in Developing Countries. *Membranes* **2022**, *12* (1), 30.
(26) Saha, P.; Wagner, T. V.; Ni, J.; Langenhoff, A. A. M.; Bruning, H.; Rijnaarts, H. H. M. Cooling Tower Water Treatment Using a Combination of Electrochemical Oxidation and Constructed Wetlands. *Process Saf. Environ. Prot.* **2020**, *144*, 42−51.
(27) Hoek, E. M. V.; Allred, J.; Knoell, T.; Jeong, B.-H. Modeling the Effects of Fouling on Full-Scale Reverse Osmosis Processes. *J. Membr. Sci.* **2008**, *314* (1), 33−49.
(28) Kim, S.; Hoek, E. M. V. Modeling Concentration Polarization in Reverse Osmosis Processes. *Desalination* **2005**, *186* (1), 111−128.
(29) Samson, E.; Marchand, J.; Snyder, K. A. Calculation of Ionic Diffusion Coefficients on the Basis of Migration Test Results. *Mater. Struct.* **2003**, *36* (3), 156−165.
(30) Mackin, J. E. The Free-Solution Diffusion Coefficient of Boron: Influence of Dissolved Organic Matter. *Mar. Chem.* **1986**, *20* (2), 131−140.
(31) Wang, Y.; Combe, C.; Clark, M. M. The Effects of pH and Calcium on the Diffusion Coefficient of Humic Acid. *J. Membr. Sci.* **2001**, *183* (1), 49−60.
(32) Hill, D. Diffusion Coefficients of Nitrate, Chloride, Sulphate and Water in Cracked and Uncracked Chalk. *J. Soil Sci.* **1984**, *35* (1), 27−33.
(33) Wollast, R.; Garrels, R. M. Diffusion Coefficient of Silica in Seawater. *Nat. Phys. Sci.* **1971**, *229* (3), 94.
(34) Zeebe, R. E. On the Molecular Diffusion Coefficients of Dissolved CO2,HCO3-, and CO32- and Their Dependence on Isotopic Mass. *Geochim. Cosmochim. Acta* **2011**, *75* (9), 2483−2498.
(35) Li, J.; Zhang, C.; Tan, H.; Zeng, M.; Cheng, Y. Occurrence and Influencing Factors of High Groundwater Manganese in the Oxbow Lakes of the Middle Reaches of Yangtze River. *J. Hydrol.* **2024**, *630*, 130713.
(36) Biedunkova, O.; Kuznietsov, P.; Korbutiak, V. Evaluation of Return Cooling Water Reuse in the Wet Cooled Power Plant to Minimise the Impact of Water Intake and Drainage. *Sustainable Chem. Environ.* **2024**, *7*, 100151.
(37) Unger, S. R.; Kilgannon, E. M.; Elliott, D. B.; Cort, K. A.; Stoughton, K. L. M. *Water and Wastewater Annual Price Escalation Rates for Selected Cities Across the United States*; PPacific Northwest National Laboratory: Richland, WA (United States), 2023. https://www.osti.gov/biblio/1975260 (accessed 2024−10−08).
(38) Uludag-Demirer, S.; Olson, N.; Ives, R.; Nshimyimana, J. P.; Rusinek, C. A.; Rose, J. B.; Liao, W. Techno-Economic Analysis of Electrocoagulation on Water Reclamation and Bacterial/Viral Indicator Reductions of a High-Strength Organic Wastewater—Anaerobic Digestion Effluent. *Sustainability* **2020**, *12* (7), 2697.
(39) Patience, G. S.; Boffito, D. C. Distributed Production: Scale-up vs Experience. *J. Adv. Manuf. Process.* **2020**, *2* (2), No. e10039.
(40) Hashim, K. S. The Innovative Use of Electrocoagulation-Microwave Techniques for the Removal of Pollutants from Water. Ph.D. Thesis, Liverpool John Moores University (United Kingdom), England, 2017. https://www.proquest.com/docview/2001390450/abstract/366489C897904842PQ/1 (accessed 2025−05−01).
(41) *Aluminium Ingot 99.7%—Best Metal Trade*. https://bestmetaltrade.com/product/aluminium-ingot-99-7-percent/(accessed 2024−04−12).
(42) Judd, S. J.; Carra, I. Low-Pressure Membrane Technology for Potable Water Filtration: True Costs. *Water Res.* **2021**, *191*, 116826.
(43) *Treasury Reporting Rates of Exchange*; U.S. Treasury Fiscal Data. https://fiscaldata.treasury.gov/datasets/treasury-reporting-rates-exchange/(accessed 2024−10−08).
(44) *Change in Discount Rate for Water Resources Planning*; Federal Register. https://www.federalregister.gov/documents/2024/12/12/2024-29263/change-in-discount-rate-for-water-resources-planning (accessed 2025−05−01).
(45) Chauhan, A.; Saini, R. P. Techno-Economic Feasibility Study on Integrated Renewable Energy System for an Isolated Community of India. *Renewable Sustainable Energy Rev.* **2016**, *59*, 388−405.
(46) Creese, R. C. *Strategic Cost Fundamentals: For Designers, Engineers, Technologists, Estimators, Project Managers, and Financial Analysts*; Synthesis Lectures on Engineering; Springer International Publishing: Cham, 2018.
(47) Bhojwani, S.; Topolski, K.; Mukherjee, R.; Sengupta, D.; El-Halwagi, M. M. Technology Review and Data Analysis for Cost Assessment of Water Treatment Systems. *Sci. Total Environ.* **2019**, *651*, 2749−2761.
(48) La Plante, E. C.; Chen, X.; Bustillos, S.; Bouissonnie, A.; Traynor, T.; Jassby, D.; Corsini, L.; Simonetti, D. A.; Sant, G. N. Electrolytic Seawater Mineralization and the Mass Balances That Demonstrate Carbon Dioxide Removal. *ACS EST Eng.* **2023**, *3* (7), 955−968.
(49) Lishchynskyi, O.; Stetsyshyn, Y.; Raczkowska, J.; Awsiuk, K.; Orzechowska, B.; Abalymov, A.; Skirtach, A. G.; Bernasik, A.; Nastyshyn, S.; Budkowski, A. Fabrication and Impact of Fouling-Reducing Temperature-Responsive POEGMA Coatings with Embedded CaCO3 Nanoparticles on Different Cell Lines. *Materials* **2021**, *14* (6), 1417.
(50) Gong, L.; Yao, Z.; Zhu, C.; Lian, X.; He, B.; Qu, L.; Xiong, W.; Yu, B. Synthesis of Porous Mg(OH)2 Nanowires for Phosphate Removal from Water. *Colloids Surf., A* **2023**, *676*, 132137.
(51) Castañeda, L. F.; Coreño, O.; Nava, J. L.; Carreño, G. Removal of Fluoride and Hydrated Silica from Underground Water by Electrocoagulation in a Flow Channel Reactor. *Chemosphere* **2020**, *244*, 125417.
(52) Castañeda, L. F.; Coreño, O.; Carreño, G.; Nava, J. L. Electrocoagulation with Fe-Al Hybrid Electrodes for the Removal of Arsenic, Fluoride, and Silica from Natural Groundwater. *Chem. Eng. Process.* **2023**, *190*, 109434.
(53) Castañeda, L. F.; Coreño, O.; Nava, J. L. Arsenic and Hydrated Silica Removal from Groundwater by Electrocoagulation Using an Up-Flow Reactor in a Serpentine Array. *J. Environ. Chem. Eng.* **2019**, *7* (5), 103353.
(54) Mahmood, M.; Yasri, N.; Fuladpanjeh-Hojaghan, B.; Roberts, E. P. L. Influence of Operating Conditions on the Removal of Silica and Hardness by Continuous Electrocoagulation. *J. Environ. Chem. Eng.* **2022**, *10* (6), 108899.
(55) Castañeda, L. F.; Coreño, O.; Nava, J. L. Simultaneous Elimination of Hydrated Silica, Arsenic and Phosphates from Real Groundwater by Electrocoagulation Using a Cascade-Shaped up-Flow Reactor. *Electrochim. Acta* **2020**, *331*, 135365.
(56) López, R. L.; Coreño, O.; Nava, J. L. Abatement of Hydrated Silica and Simultaneous Removal of Coexisting Ions from Deep Well Water by Electrocoagulation Using an Up-Flow Reactor. *J. Water Process Eng.* **2019**, *32*, 100923.
(57) Kim, S.; Lee, M.; Choi, S.; Won, J.; Kim, T.; Kim, T.; Bae, J.; Shim, W. Cation-Selective Layered Silicon Oxide Membranes for Power Generation. *J. Phys. Energy* **2023**, *5* (1), 014010.
(58) Yuan, Z.; Lu, M.; Peng, X.; Xu, B.; Shi, Y.; Zhao, H. Performance and Purification Mechanism of the Mullite/SiC Composite Filter Tube Membrane. *Process. Appl. Ceram.* **2023**, *17* (1), 61−69.
(59) Lewis, W. J. T.; Mattsson, T.; Chew, Y. M. J.; Bird, M. R. Investigation of Cake Fouling and Pore Blocking Phenomena Using Fluid Dynamic Gauging and Critical Flux Models. *J. Membr. Sci.* **2017**, *533*, 38−47.

https://doi.org/10.1021/acsestengg.5c00537
ACS EST Engg. XXXX, XXX, XXX−XXX

(60) Lan, Y.; Groenen-Serrano, K.; Coetsier, C.; Causserand, C. Fouling Control Using Critical, Threshold and Limiting Fluxes Concepts for Cross-Flow NF of a Complex Matrix: Membrane BioReactor Effluent. *J. Membr. Sci.* **2017**, *524*, 288−298.
(61) Algurainy, Y.; Call, D. F. Cathodic Precipitation of Calcium Carbonate and Its Impact on the Electrosorption of Sodium in Flow-through Capacitive Deionization. *Desalination* **2024**, *586*, 117853.
(62) Donneys-Victoria, D.; Marriaga-Cabrales, N.; Machuca-Martínez, F.; Benavides-Guerrero, J.; Cloutier, S. G. Indigo Carmine and Chloride Ions Removal by Electrocoagulation. Simultaneous Production of Brucite and Layered Double Hydroxides. *J. Water Process Eng.* **2020**, *33*, 101106.
(63) Benecke, J. *Gypsum Scaling During Reverse Osmosis Desalination - Characterization and Effects of Natural Organic Matter*; Technischen Universität Hamburg, 2018. http://tubdok.tub.tuhh.de/handle/11420/1838 (accessed 2025−05−06).
(64) Cherif, H.; Labbaoui, A.; Risse, H.; Boughanmi, H.; Elfil, H. Magnesium Recovery from Brackish Water Desalination Brine and Valorization in Fertilizer Production. *J. Environ. Chem. Eng.* **2024**, *12* (5), 113799.
(65) Lee, H.-J.; Halali, M. A.; Baker, T.; Sarathy, S.; de Lannoy, C.-F. A Comparative Study of RO Membrane Scale Inhibitors in Wastewater Reclamation: Antiscalants versus pH Adjustment. *Sep. Purif. Technol.* **2020**, *240*, 116549.
(66) Davood Abadi Farahani, M. H.; Borghei, S. M.; Vatanpour, V. Recovery of Cooling Tower Blowdown Water for Reuse: The Investigation of Different Types of Pretreatment Prior Nanofiltration and Reverse Osmosis. *J. Water Process Eng.* **2016**, *10*, 188−199.
(67) Panagopoulos, A.; Haralambous, K.-J.; Loizidou, M. Desalination Brine Disposal Methods and Treatment Technologies - A Review. *Sci. Total Environ.* **2019**, *693*, 133545.
(68) Ziolkowska, J. R.; Reyes, R. Chapter 3.1.3 - Prospects for Desalination in the United States—Experiences From California, Florida, and Texas. In *Competition for Water Resources*; Ziolkowska, J. R., Peterson, J. M., Eds.; Elsevier, 2017; pp 298−316.
(69) Veil, J.; Hanson, G.; Hayes, T.; Mantell, M.. In *Proceedings of the Technical Workshops for the Hydraulic Fracturing Study: Water Resources Management*; US Environmental Protection Agency, Office of Research and Development, 2011.
(70) Soliman, M.; Eljack, F.; Kazi, M.-K.; Almomani, F.; Ahmed, E.; El Jack, Z. Treatment Technologies for Cooling Water Blowdown: A Critical Review. *Sustainability* **2022**, *14* (1), 376.
(71) Amoatey, P.; Izady, A.; Al-Maktoumi, A.; Chen, M.; Al-Harthy, I.; Al-Jabri, K.; Msagati, T. A. M.; Nkambule, T. T. I.; Baawain, M. S. A Critical Review of Environmental and Public Health Impacts from the Activities of Evaporation Ponds. *Sci. Total Environ.* **2021**, *796*, 149065.
(72) von Eiff, D.; Wong, P. W.; Gao, Y.; Jeong, S.; An, A. K. Technical and Economic Analysis of an Advanced Multi-Stage Flash Crystallizer for the Treatment of Concentrated Brine. *Desalination* **2021**, *503*, 114925.
(73) *Electric Power Monthly*; U.S. Energy Information Administration. https://www.eia.gov/electricity/monthly/epm_table_grapher.php (accessed 2024−10−15).
(74) Ayres, D.; Zamora, L. *Renewable Power Generation Costs in 2023*; International Renewable Energy Agency: Abu Dhabi, 2024.

https://doi.org/10.1021/acsestengg.5c00537
ACS EST Engg. XXXX, XXX, XXX−XXX